Investigation of the Performance of Different Loss Function Types Within Deep Neural Anchor-Free Object Detectors

Ala'a Alshubbak[1,2] and Daniel Görges[1]
[1]Institute of Electromobility, University of Kaiserslautern-Landau, Kaiserslautern, Germany
[2]German Jordanian University, Amman, Jordan

Keywords: Anchor-Free Object Detection, Deep Learning, ResNet, IOU Losses, Attention Mechanism, Saliency Map.

Abstract: In this paper, an investigation of different IoU loss functions and a spatial attention mechanism within anchor-free object detectors is presented. Two anchor-free dense predictor models are studied: FASF and FCOS models. The models are tested on two different datasets: the benchmark COCO dataset and a small dataset called OPEDD. The results show that some loss functions and using the attention mechanism outperform their original counterparts for both the huge multi-class COCO dataset and the small unity-class dataset of OPEDD. The proposed structure is tested over different backbones: ResNet-50, ResNet-101, and ResNeXt-101. The accuracy of basic models trained over the coco dataset improves by 1.3% and 1.6% mAP for the FSAF and FCOS models based on ResNet-50, respectively. On the other hand, it increases by 2.3% and 15.8% for the same models when trained on the OPEDD dataset. The effect is interpreted using a saliency map.

1 INTRODUCTION

Deep learning is a new machine learning technique that uses deep neural networks to perform various tasks e.g in robotics, natural language processing, and image recognition. In computer vision, these networks are trained on large datasets to learn patterns and features in visual data, enabling them to perform tasks such as object detection, image classification, and segmentation. By leveraging the representational power and robustness of deep learning models, computer vision applications can achieve state-of-the-art performance.

Deep learning-based object detection is divided into two approaches: anchor-free and anchor-based detectors (Liu et al., 2020). Anchor-free detectors are different from anchor-based ones in the technique used to produce the boundary box of objects. The latter approach relies on pre-defined anchor boxes, while the first one uses mostly multi-level Feature Pyramid Network (FPN) (Lin et al., 2017a) prediction to extract the necessary features for each object. The anchor-based approach is considered the more accurate one, but with some disadvantages. It is more complex and requires more time in the training phase. On the other hand, an anchor-free approach is a new approach that gets rid of some problems present in the previous approach, such as creating multi-proposed regions and the imbalance between negative and positive samples.

Anchor-free detectors are still an emerging area of research and worth investigating further. Relatively little effort has been spent so far in improving the performance of anchor-free detectors and deploying them in real-time applications. In this work, two of the anchor-free dense predictors are used, the Feature Selective Anchor-Free Module (FSAF) (Zhu et al., 2019a) and the Fully Convolutional One-Stage Object Detection (FCOS) (Tian et al., 2019), as those two models are the most popular dense models that are based on both FPN and Intersection over Union (IoU) loss for bounding box regression. In this paper the effect of using different types of IoU losses within the anchor-free dense predictors is investigated, with a focus on applications in rural environments, which has rarely been discussed before. Figure 1 shows the general structure of such dense anchor-free models. In the investigations the spatial attention mechanism (Zhu et al., 2019b) is included within the backbone of the models to enhance their performance. It is shown that by using such technique, anchor-free dense predictors can be improved depending on to their structure by 0.8% and 0.4% mAP for FSAF and FCOS ResNet-50 models, respectively. Moreover this improvement does not increase the complexity of the original deep neural network model.

Alshubbak, A. and Görges, D.
Investigation of the Performance of Different Loss Function Types Within Deep Neural Anchor-Free Object Detectors.
DOI: 10.5220/0012354900003636

In *Proceedings of the 16th International Conference on Agents and Artificial Intelligence (ICAART 2024) - Volume 3*, pages 401-411
ISBN: 978-989-758-680-4; ISSN: 2184-433X

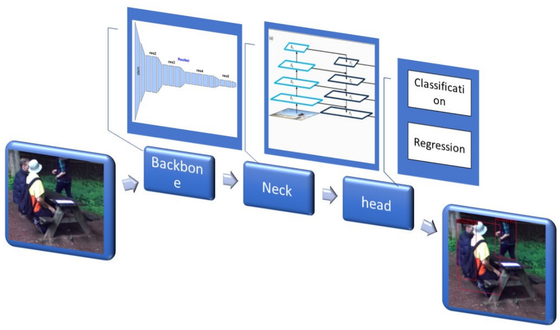

Figure 1: General structure of dense anchor-free model.

The paper is divided into five sections: the first one introduces previous work while the second one describes the architecture of the proposed approach. The third section explains the setup of the environment, the datasets, and the evaluation criteria. The results and discussion section provides a detailed explanation of the performance of the proposed approach. Lastly, future directions are discussed.

2 RELATED WORK

Much previous work has focused on detecting humans in urban environments using various datasets such as KITTI (Geiger et al., 2012), Caltech (Dollár et al., 2009) Pedestrian Detection, and Oxford (Maddern et al., 2017). However, the detection of humans in rural environments remains a challenging task, with fewer datasets and less effort put into this field. The rural environment is highly unstructured, and its characteristics are different from those of urban environments, making it more challenging to detect humans. Table 1 shows a detailed comparison between the two environments in terms of detecting humans. Three approaches are reported in literature to detect humans in orchards and suburban environments, including classical machine learning approaches such as rigid object detectors and deformable parts models, as well as deep convolutional neural network models. Most of the state-of-the-art object detectors based on deep neural networks have been trained on benchmark datasets such as COCO (Lin et al., 2014). Relying on transfer learning between urban and rural environments leads to low-performance results, and researchers have had to train new models with new datasets from the rural domain (Neigel et al., 2020; Neigel et al., 2021).

The focus of this paper is to investigate models that are based on a deep learning (DL) approach with a less complex structure and enhance their performance and speed to compete with existing detectors.

Table 1: Difference between urban environment and suburban or rural environment in the detection of humans (Jiang et al., 2021; Xiang et al., 2020; Kragh et al., 2017).

Items	Urban environment	Suburban environment
Human Pose	Limited poses, such as walking, standing, and riding a bike.	More challenging poses, such as jumping, crouching, lying, and bending.
HOG Visualization	Non-uniform, easy to discover different patterns.	Uniform patterns, have repetitive texture.
Datasets	Rich & multiple datasets: KITTI, Caltech-USA, Oxford dataset .	Fewer datasets, such as RELLIS-3D (Jiang et al., 2021), OPEDD (Neigel et al., 2020), FieldSAFE (Kragh et al., 2017), and KIT MOMA(Xiang et al., 2020).
Problem	Mostly dense objects	More partially occluded, dense and small objects
Background Characteristic	Low texture, represented by horizontal and vertical edges.	More complex texture distributed over different orientations.
Content Relation	More contextual information	Less contextual information.
Detector Paradigm	Traditional methods (SVM, DPM) and DL	Less work, mostly DL with sensor fusion (Jiang et al., 2021)

According to that, only anchor-free detectors are used and tested with a small, specific dataset as well as a benchmark dataset, which will enhance the reliability of the proposed approach.

3 MODEL ARCHITECTURE

3.1 Model Structure

The architecture of object detectors mainly consists of three components: the backbone, the neck, and the head. The first two parts are responsible of feature extraction, while the head part is used for classification and regression of an object and its bounding box. Dense anchor-free detectors share the same structure using a backbone from the ResNet family (He et al., 2016; Xie et al., 2017) and a neck using FPN (Lin et al., 2017a).

The FSAF and FCOS models used in this paper are different in the way of regression of the bounding boxes of the objects in their head part. The FSAF model uses the idea of a 4-dimensional vector for regression, while the FCOS model uses a centerness loss to adjust the bounding box according to the center of the object. Both of these models use focal loss (Lin et al., 2017b) for classification.

3.2 Loss Functions

In object detection models, two types of loss functions are used: one for classification and another for regression of bounding boxes. Cross-entropy loss is mostly used in anchor-based detectors for classification, while focal loss is used in anchor-free detectors. Regression loss is used to optimize the position of the bounding boxes and smooth L1 loss or cross-entropy loss is used in anchor-based detectors, while Intersection over Union (IoU) loss (Yu et al., 2016) is used in dense predictors. Recently, modifications have been proposed for IoU loss to improve its performance, including GIoU (Rezatofighi et al., 2019), DIoU, and CIoU loss (Zheng et al., 2020). The general definition of the Intersection over Union (IoU) loss is

$$IoUloss = 1 - \frac{intersection(Bb_{Predict}, Bb_{Ground})}{union(Bb_{Predict}, Bb_{Ground})} \quad (1)$$

where $Bb_{Predict}$ is the bounding box of prediction while Bb_{Ground} is the bounding box of ground truth. The modifications of IoU loss for improving its performance are defined by

1. Generalized IoU (GIoU) (Rezatofighi et al., 2019)

$$G_{IoU} = 1 - IoU + \frac{|c \setminus union(Bb_{Predict}, Bb_{Ground})|}{|c|} \quad (2)$$

   where c is the smallest enclosing object covering both $Bb_{Predict}$ and Bb_{Ground}.

2. Distance IoU (DIoU) (Zheng et al., 2020)

$$D_{IoU} = 1 - IoU + R_{DIoU} \quad (3)$$

   where R_{DIoU} is a penalty term of the central distance

$$R_{DIoU} = \frac{\rho^2(b_{Predict}, b_{Ground})}{c^2} \quad (4)$$

   where $b_{Predict}$ and b_{Ground} are the central points of Bb_{Ground} and $Bb_{Predict}$, ρ is the Euclidean distance between the two center points, and c is the diagonal length of the smallest enclosing box covering the two boxes. Figure 2 shows all parameters that are used in the adjustment of DIoU loss regression.

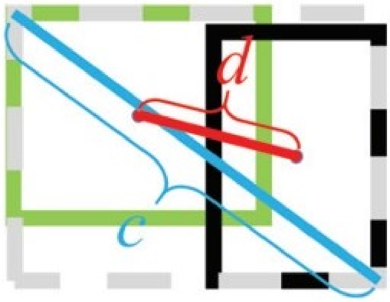

Figure 2: DIoU loss function representation with distance d between central points of ground truth box (green) and predicted box (black) and c as diagonal length of the smallest enclosing box (grey) that covers those two boxes (Zheng et al., 2020).

3. Complete IoU (CIoU) (Zheng et al., 2020)

$$C_{IoU} = D_{IoU} + \alpha\upsilon \quad (5)$$

   where α is a trade-off parameter and υ is the aspect ratio which are described by

$$\upsilon = \frac{4}{\pi^2}\left(\arctan\frac{w_{gt}}{h_{gt}} - \arctan\frac{w}{h}\right)^2 \quad (6)$$

$$\alpha = \frac{\upsilon}{(1 - IoU) + \upsilon} \quad (7)$$

   where w_{gt} and h_{gt} are the width and height of the ground truth bounding box and w and h are the width and height of the predicted bounding box.

The main difference between these losses is the introduction of new terms, such as central point distance, overlap area, and aspect ratio. Most research in anchor-based detectors shows that systems using CIoU loss converge faster and provide more accurate object localization results. The investigation of different IoU losses within anchor-free detectors has not been covered yet. It is the topic of this paper.

3.3 Attention Mechanism

The attention mechanism has been inspired by the human visual system (Guo et al., 2022) with which humans can understand what is in the scene and where it is from the initial glance. Essentially, deep neural network researchers try to further improve the performance of CNNs by adding mechanisms to answer questions such as what to pay attention to (channel attention), where to pay attention (spatial attention), when to pay attention (temporal attention), and which to pay attention to (branch attention).

In this paper, a spatial attention mechanism (Zhu et al., 2019b) in a plug-in manner is used instead of using a combination of channel and spatial ones as most researchers mention that a spatial attention mechanism is suited for dense prediction situations, while channel attention is rather used for classification tasks (Guo et al., 2022).

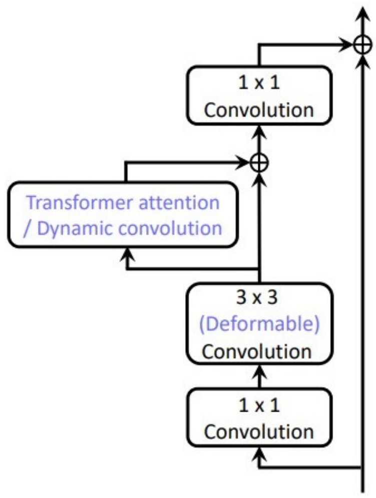

Figure 3: Plug-in attention block in purple within the residual block in ResNet (Zhu et al., 2019b).

The spatial attention mechanism in general has four main factors from which the attention model assigns weights to the key with respect to the query (Zhu et al., 2019b). Those factors are (i) the query and key content ε1, (ii) the query content and relative position ε2, (iii) the key content only ε3, and (iv) the relative position only ε4.

This attention layer has been added into two stages within the ResNet-50 model: stage 4 (Residual Block 4) and stage 5 (Residual Block 5). Its exact location is shown in Figure 3, which is between the 3x3 convolutional layer and the 1x1 convolutional layer for all residual blocks in both stage 4 and stage 5.

Our model uses the factor of key content only (ε3) which generates higher performance. Figure 4 shows the modified structure of the proposed model after adding the spatial attention block and with the loss functions.

4 DATASETS AND TRAINING ENVIRONMENT

4.1 Dataset and Evaluation Criteria

Different datasets have been produced in the field of agriculture as well as suburban and rural settings, even though those datasets are still fewer than the ones used to detect and recognize objects in urban settings. In this paper, the dataset OPEDD (Neigel et al.,

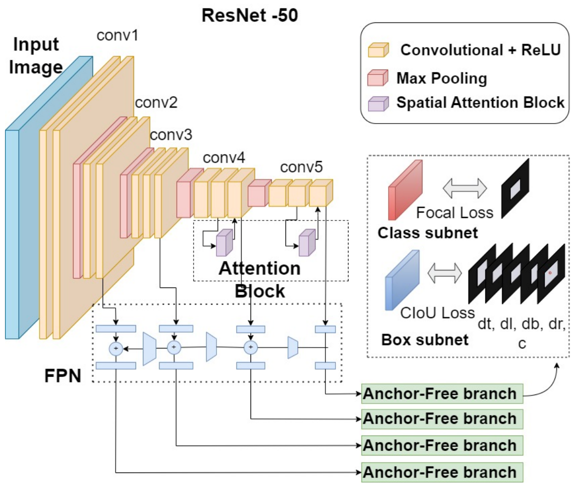

Figure 4: Modified structure of the FSAF model that used in this work.

2020) is used, which consists of two types of suburban environments: meadow areas or construction areas. It consists of 1018 images captured by a stereo camera. 845 images are used for training purposes, 88 images for testing and 82 images for validation. All samples contain at least one human as a major category to be detected.

Three main evaluation parameters are used in this investigation: the mean average precision (mAP), the floating-point operations FLOPs (GFLOPs), and trained parameters as well as the average iteration time (seconds per iteration).

The mean average precision is a representation of the accuracy of the model while the iteration time is an indication of training speed. On the other hand, the FLOPs and trained parameters give an initial indication of the complexity of each model. This factor is not so accurate, as it does not include the attention mechanism layers. Table 2 shows the FLOPs and the parameters for different models for comparison. The bar charts in Figure 5 show the differences in average iteration time for different anchor-free model structures for both FSAF and FCOS models.

All methods presented in this paper are tested for three main sizes of the object (small, medium, and large) and under different threshold values for Intersection over Union (IoU) (50% and 75%). Tables 3, 4, and 5 show the performance of each of the models used in this paper and the effect of using the spatial attention mechanism within the structure.

4.2 Training Environment

The experiments are carried out on a machine with one NVIDIA RTX A6000 GPU using the ResNet family (He et al., 2016; Xie et al., 2017) for dense

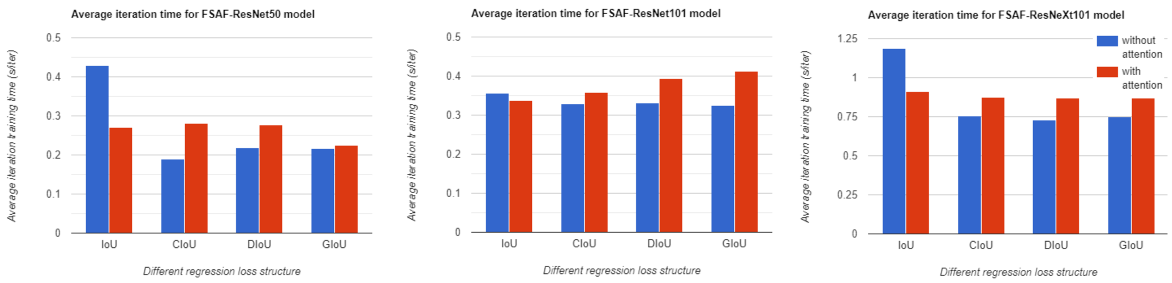

(a) The FSAF model

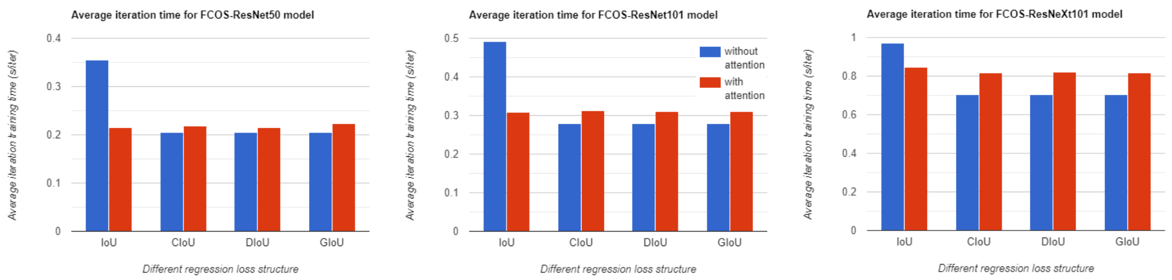

(b) The FCOS model

Figure 5: Average iteration time for both the FSAF and FCOS models with different structures trained on the COCO benchmark dataset.

Table 2: Complexity measurements for both FSAF and FCOS model with different backbone structures with and without Spatial Attention Mechanisms.

Model	Backbone	Structue	Complexity	
			Flops	Param
FSAF	ResNet-50	w/o att	206.28	36.19
		w att	207.48	39.74
	ResNet-101	w/o att	282.35	55.19
		w att	285.8	62.08
	ResNeXt-101	w/o att	439.57	93.92
		w att	494.49	204.08
FCOS	ResNet-50	w/o att	200.55	32.02
		w att	201.75	35.56
	ResNet-101	w/o att	276.62	50.96
		w att	280.07	57.86
	ResNeXt-101	w/o att	438.59	89.79
		w att	493.5	199.95

detectors (Kong et al., 2020; Tian et al., 2019; Zhu et al., 2019a). The original resolution of the input images is 2208 x 1242, which is changed into different sizes, mainly 1333 x 800 for anchor-free dense predictors. The model is trained over 12 epochs for the COCO benchmark dataset and over 30 epochs for the OPEDD dataset. All models are trained on a batch size of 2 except the FSAF model trained over the OPEDD dataset where a batch size of 4 is used. The MMDetection open-source toolbox (Chen et al., 2019) is partially used to design the modified model and plug in the attention mechanism block.

5 RESULTS AND DISCUSSION

5.1 Performance of Models on OPEDD Dataset

The main result is presented in Table 3. It shows a comparison in Mean Average Precision (mAP) between baseline structures of both FSAF and FCOS dense object detectors and our proposed structures. It is obviously seen that using the CIoU loss with the spatial attention mechanism in an anchor-free detector improves the detection accuracy with 2.3 % mAP compared to the baseline structure of the FSAF model. Additionally, it shows an increase of 16.1% mAP compared to the baseline structure of the FCOS model. Moreover, the result shows that the changes within the structure and architecture of the FSAF model enhance the detection of small objects which is one of the challenging topics in computer vision and object detection (Tong et al., 2020). The proposed approach enhances the detection of small, medium, and large objects by 2.8%, 5.9%, and 1.6% mAP respectively. Corresponding results are obtained for the FCOS model with a ratio of 2.9%, 11.9%, and 35.6% mAP, respectively.

Further analysis is mentioned in Table 4. A baseline structure for both FSAF and FCOS models pretrained on a benchmark COCO dataset is used as a transfer learning stage for training all new proposed structures on the OPEDD dataset. The results show that the modified structure with spatial attention and GIoU loss outperforms the baseline structure by 0.4% for the FSAF model and by 0.7% for the FCOS model.

Figure 6 shows exemplary results of detecting humans using dense predictors. The figure illustrates the improvement of the proposed FSAF model with the new structure over the original structure as well as over other dense predictor structures such as FoveaBox (Kong et al., 2020) and FCOS all of which have the same backbone of ResNet-50 (He et al., 2016). It is noticeable that both the FSAF and FCOS models in their original structure which contains an IOU loss can not detect humans in occluded situations, while the proposed modification in the FSAF model makes it more accurate without huge changes in the deep structure of the neural network.

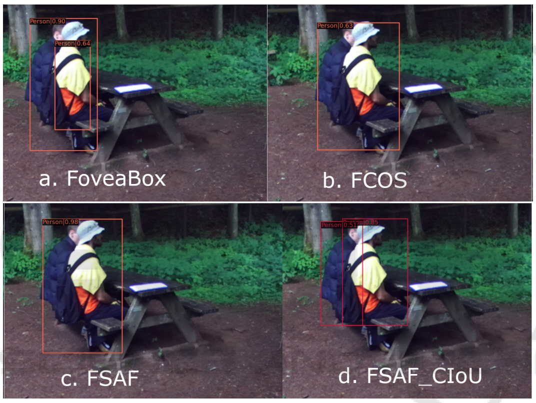

Figure 6: Results of detecting a human in a dense (occluded) situation using different dense predictors, a. FoveaBox, b. FCOS, c. FSAF with normal IoU loss, and d. new FSAF structure with an attention mechanism. All models have the backbone of ResNet-50. .

5.2 Saliency Map for an Explanation of Deep Neural Network Behavior

A saliency map is a technique used to highlight the most important features in computer vision that affect the detection process. The D-RISE saliency map (Petsiuk et al., 2021) is used in this work to give a clear overview of what is going on behind the models and their structure. It shows how each model looks at the features within the images, and how to detect each category. The D-RISE approach has been chosen over other saliency methods as it has the ability to explain different types of object detectors, both one-stage and two-stage detectors. Figure 7 shows the different saliency maps produced after changing the FCOS ResNeXt-101 and FSAF ResNet-50 models. The saliency maps of the ResNeXt backbone model are darker and more accurate as the model is deeper with a huge number of layers in its backbone.

5.3 Ablation Study

In order to assess the reliability of the proposed structures, the proposed modifications are designed with both FSAF and FCOS and tested with the huge benchmark COCO dataset. The results of two different backbones are recorded and compared with the original structure. Table 5 contains the accuracy of FSAF and FCOS with a ResNet-50 backbone, respectively. The results show that both models that have DIoU and CIoU losses give the most accurate results in comparison with the theoretical baseline structures, even when changing the backbone from ResNet-50 to a deeper one such as ResNeXt-101 (see Appendix A). The modification structures show an increasing of mAP by 1.3% for FSAF model and 1.6% for the FCOS model. Figure 8 presents some results of the FCOS model trained on the COCO dataset with different IoU loss functions. It shows that the model with DIoU detects more objects and enhances the detection of occluded objects such as humans in the same image. More results of different structures with different backbones are given in Appendix A.

6 CONCLUSION AND FUTURE DIRECTIONS

The paper discusses the use of object detection in rural and suburban areas. It summarizes the existing efforts to detect objects efficiently and describes the datasets and state-of-the-art anchor-free models used in this field. Furthermore, new anchor-free model structures are investigated based on different types of regression losses. Training over the benchmark COCO dataset with both FSAF and FCOS ResNet-50 models based on CIOU and a spatial attention mechanism shows an improvement of the accuracy by 1.3 % and 1.6 % mAP, respectively. The object detection results with different structures have been interpreted using a saliency map, which shows the area at which each model is focused to discover and detect the necessary object. On the other hand, the modified structures have been investigated using a specific dataset from construction fields (OPEDD). The results show that structure based on spatial attention and CIoU loss for both FSAF and FCOS models increase the accuracy by 2.3% and 16.1% mAP respectively.

Moreover, in a comparison between such approaches and the State-Of-the-Art (SOTA) YOLO object detection versions, the results show that the

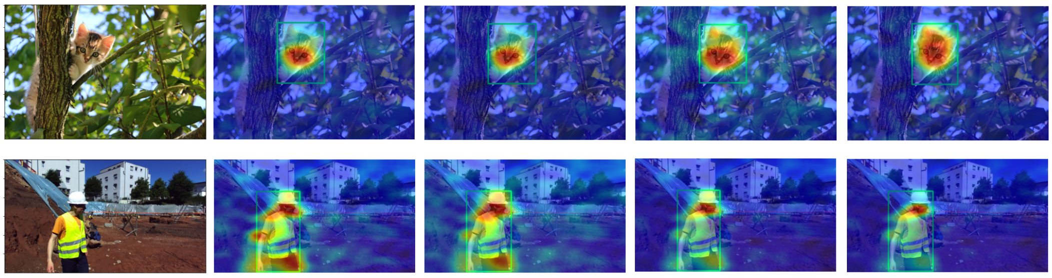

a. original image. b. saliency map for normal FCOS model. c. saliency map for FCOS CIoU att model. d. saliency map for FCOS DIoU att model. e. saliency map for FCOS GIoU att model.

(a) FCOS ResNeXt-101 saliency maps

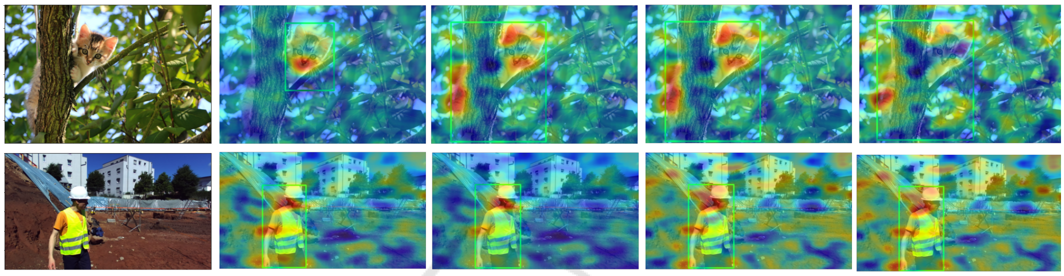

a. Original image. b. saliency map for normal FSAF model. c. saliency map for FSAF CIoU att model. d. saliency map for FSAF DIoU att model. e. saliency map for FSAF GIoU att model.

(b) FSAF ResNet-50 saliency maps

Figure 7: The saliency maps for different models that are tested in this research.

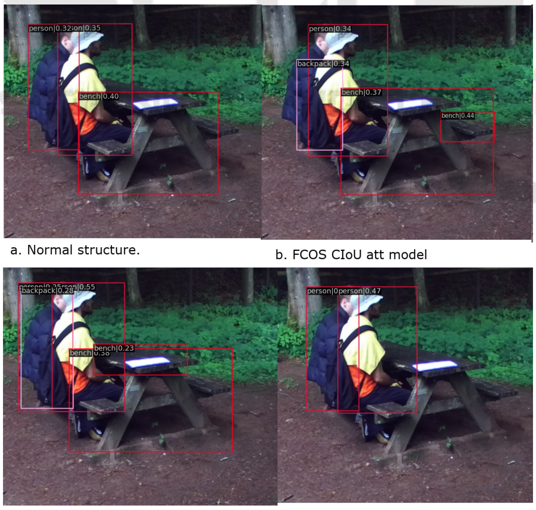

a. Normal structure. b. FCOS CIoU att model c. FCOS DIoU att model d. FCOS GIoU att model

Figure 8: Object detection results for different structures of FCOS ResNeXt-101 model trained on COCO dataset.

anchor-free models with such a modification give FLOPs values less or slightly higher than YOLO models. For example, the literature mentions that the YOLOv5x (Jocher, 2020) has a FLOPs value of 205.7, and the one for YOLOv8x (Hussain, 2023) is 257.8, while the FLOPs for both the FSAF and the FCOS model based on ResNet-50 mentioned in Table 2 are 207.48 and 201.75; respectively. Even though those models have inherited an attention mechanism in their structure. More detailed results for different backbone structures in both the FSAF and FCOS models are mentioned in Appendix A and B. Those results prove that using either CIoU and DIoU losses with attention gives more accurate results compared to the theoretical baseline structure with IoU loss.

For future work, more anchor-free detectors can be investigated for the different types of loss functions and different types of attention mechanisms such as the convolutional block attention module (CBAM) (Woo et al., 2018) which could enhance their performance and accuracy with less change in complexity. From the authors' point of view, anchor-free models are still a springboard for future research. They can be developed in a semi-supervised approach as well. Models that contain FPN in their structure are more compatible with the future direction toward biological plausibility (Helmstaedter, 2015).

ACKNOWLEDGEMENTS

This research was supported by German Academic Exchange Service (DAAD).

Table 3: Performance of different structures of dense object detectors: FSAF and FCOS models based on ResNet50 backbone trained directly on the OPEDD dataset. The highest values are mentioned in bold.

Model	Backbone	Attention	Reg loss	Bbox-mAP	Bbox-mAP-50	Bbox-mAP-75	Bbox-mAP-s	Bbox-mAP-m	Bbox-mAP-l
Anchor-Free Detectors: Dense Predictors									
FSAF	ResNet-50	Baseline	IoU	22.7	36.1	24.8	5.5	36.5	30.0
		ε3(our)	IoU	24.8	**39.0**	26.4	8.0	40.8	31.1
		ε3(our)	CIoU	**25.0**	38.4	26.6	**8.3**	**42.4**	**31.6**
		ε3(our)	DIoU	24.7	38.5	**27.5**	7.0	41.8	31.2
		ε3(our)	GIoU	24.4	**39.0**	26.8	6.3	41.7	31.1
FCOS	ResNet-50	Baseline	IoU	13.6	28.8	11.2	1.1	12.5	22.6
		ε3(our)	IoU	24.5	50.1	23.8	1.3	23.9	44.6
		ε3(our)	CIoU	**29.7**	**54.8**	**30.7**	**4.0**	**24.4**	**58.2**
		ε3(our)	DIoU	28.9	54.3	29.9	3.8	23.9	56.9
		ε3(our)	GIoU	27.6	51.2	27.0	1.7	22.8	56.3

Table 4: Performance of different structures of dense object detectors: FSAF and FCOS models based on ResNet50 backbone pre-trained on COCO dataset, then transfer learning using the OPEDD dataset. The highest values are mentioned in bold.

Model	Backbone	attention	Reg loss	Bbox-mAP	Bbox-mAP-50	Bbox-mAP-75	Bbox-mAP-s	Bbox-mAP-m	Bbox-mAP-l
Anchor-Free Detectors: Dense Predictors									
FSAF	ResNet-50	N	IoU	24.1	35.9	**26.8**	6.7	41.1	31.6
		ε3(our)	IoU	**24.5**	**38.2**	25.5	7.6	39.5	**32.0**
		ε3(our)	CIoU	24.1	37.4	26.5	**9.2**	40.7	30.5
		ε3(our)	DIoU	23.4	35.7	24.7	6.1	**42.0**	29.0
		ε3(our)	GIoU	**24.5**	37.3	**26.8**	7.9	38.4	31.8
FCOS	ResNet-50	N	IoU	24.9	37.0	25.9	3.4	38.2	34.1
		ε3(our)	IoU	23.7	36.3	25.8	3.1	35.7	32.5
		ε3(our)	CIoU	24.8	37.8	26.8	3.9	37.3	34.2
		ε3(our)	DIoU	25.4	**39.2**	**27.1**	**4.7**	38.1	**34.9**
		ε3(our)	GIoU	**25.6**	**39.2**	26.9	**4.7**	**39.9**	34.6

Table 5: Performance of different structures of dense object detectors: FSAF and FCOS models based on ResNet50 backbone trained on the benchmark COCO dataset. The highest values are mentioned in bold.

Model	Backbone	Attention	Reg loss	Bbox-mAP	Bbox-mAP-50	Bbox-mAP-75	Bbox-mAP-s	Bbox-mAP-m	Bbox-mAP-l
Anchor-Free Detectors: Dense Predictors									
FSAF	ResNet-50	N	IoU	36.0	55.5	37.7	19.6	39.6	48.2
		ε3(our)	IoU	36.3	55.4	38.6	20.1	39.4	47.7
		ε3(our)	CIoU	**37.3**	56.8	39.2	21.1	40.0	**49.0**
		ε3(our)	DIoU	**37.3**	**56.9**	39.2	**21.2**	**40.1**	48.6
		ε3(our)	GIoU	37.2	56.4	**39.6**	21.0	40.0	**49.0**
FCOS	ResNet-50	N	IoU	36.6	56.0	38.8	21.1	40.7	47.1
		ε3(our)	IoU	37.4	56.3	40.0	21.6	41.1	49.0
		ε3(our)	CIoU	**38.2**	**57.1**	**40.6**	21.5	**42.1**	**50.0**
		ε3(our)	DIoU	37.8	56.8	40.2	22.0	41.7	49.4
		ε3(our)	GIoU	38.1	56.9	40.5	**22.3**	41.9	49.7

REFERENCES

Chen, K., Wang, J., Pang, J., Cao, Y., Xiong, Y., Li, X., Sun, S., Feng, W., Liu, Z., Xu, J., et al. (2019). Mmdetection: Open mmlab detection toolbox and benchmark. *arXiv preprint arXiv:1906.07155*.

Dollár, P., Wojek, C., Schiele, B., and Perona, P. (2009). Pedestrian detection: A benchmark. In *2009 IEEE Conference on Computer Vision and Pattern Recognition*, pages 304–311. IEEE.

Geiger, A., Lenz, P., and Urtasun, R. (2012). Are we ready for autonomous driving? the kitti vision benchmark suite. In *2012 IEEE conference on computer vision and pattern recognition*, pages 3354–3361. IEEE.

Guo, M.-H., Xu, T.-X., Liu, J.-J., Liu, Z.-N., Jiang, P.-T., Mu, T.-J., Zhang, S.-H., Martin, R. R., Cheng, M.-M., and Hu, S.-M. (2022). Attention mechanisms in computer vision: A survey. *Computational Visual Media*, pages 1–38.

He, K., Zhang, X., Ren, S., and Sun, J. (2016). Deep residual learning for image recognition. In *Proceedings of the IEEE conference on computer vision and pattern recognition*, pages 770–778.

Helmstaedter, M. (2015). The mutual inspirations of machine learning and neuroscience. *Neuron*, 86(1):25–28.

Hussain, M. (2023). Yolo-v1 to yolo-v8, the rise of yolo and its complementary nature toward digital manufacturing and industrial defect detection. *Machines*, 11(7):677.

Jiang, P., Osteen, P., Wigness, M., and Saripalli, S. (2021). Rellis-3d dataset: Data, benchmarks and analysis. In *2021 IEEE International Conference on Robotics and Automation (ICRA)*, pages 1110–1116. IEEE.

Jocher, G. (2020). Yolov5 by ultralytics.

Kong, T., Sun, F., Liu, H., Jiang, Y., Li, L., and Shi, J. (2020). Foveabox: Beyound anchor-based object detection. *IEEE Transactions on Image Processing*, 29:7389–7398.

Kragh, M. F., Christiansen, P., Laursen, M. S., Larsen, M., Steen, K. A., Green, O., Karstoft, H., and Jørgensen, R. N. (2017). Fieldsafe: dataset for obstacle detection in agriculture. *Sensors*, 17(11):2579.

Lin, T.-Y., Dollár, P., Girshick, R., He, K., Hariharan, B., and Belongie, S. (2017a). Feature pyramid networks for object detection. In *Proceedings of the IEEE conference on computer vision and pattern recognition*, pages 2117–2125.

Lin, T.-Y., Goyal, P., Girshick, R., He, K., and Dollár, P. (2017b). Focal loss for dense object detection. In *Proceedings of the IEEE international conference on computer vision*, pages 2980–2988.

Lin, T.-Y., Maire, M., Belongie, S., Hays, J., Perona, P., Ramanan, D., Dollár, P., and Zitnick, C. L. (2014). Microsoft coco: Common objects in context. In *European conference on computer vision*, pages 740–755. Springer.

Liu, S., Zhou, H., Li, C., and Wang, S. (2020). Analysis of anchor-based and anchor-free object detection methods based on deep learning. In *2020 IEEE International Conference on Mechatronics and Automation (ICMA)*, pages 1058–1065. IEEE.

Maddern, W., Pascoe, G., Linegar, C., and Newman, P. (2017). 1 year, 1000 km: The oxford robotcar dataset. *The International Journal of Robotics Research*, 36(1):3–15.

Neigel, P., Ameli, M., Katrolia, J., Feld, H., Wasenmüller, O., and Stricker, D. (2020). Opedd: Off-road pedestrian detection dataset.

Neigel, P., Rambach, J. R., and Stricker, D. (2021). Offsed: Off-road semantic segmentation dataset. In *VISIGRAPP (4: VISAPP)*, pages 552–557.

Petsiuk, V., Jain, R., Manjunatha, V., Morariu, V. I., Mehra, A., Ordonez, V., and Saenko, K. (2021). Black-box explanation of object detectors via saliency maps. In *Proceedings of the IEEE/CVF Conference on Computer Vision and Pattern Recognition*, pages 11443–11452.

Rezatofighi, H., Tsoi, N., Gwak, J., Sadeghian, A., Reid, I., and Savarese, S. (2019). Generalized intersection over union: A metric and a loss for bounding box regression. In *Proceedings of the IEEE/CVF Conference on Computer Vision and Pattern Recognition*, pages 658–666.

Tian, Z., Shen, C., Chen, H., and He, T. (2019). Fcos: Fully convolutional one-stage object detection. In *Proceedings of the IEEE/CVF international conference on computer vision*, pages 9627–9636.

Tong, K., Wu, Y., and Zhou, F. (2020). Recent advances in small object detection based on deep learning: A review. *Image and Vision Computing*, 97:103910.

Woo, S., Park, J., Lee, J.-Y., and Kweon, I. S. (2018). Cbam: Convolutional block attention module. In *Proceedings of the European conference on computer vision (ECCV)*, pages 3–19.

Xiang, Y., Wang, H., Su, T., Li, R., Brach, C., Mao, S. S., and Geimer, M. (2020). Kit moma: A mobile machines dataset. *arXiv preprint arXiv:2007.04198*.

Xie, S., Girshick, R., Dollár, P., Tu, Z., and He, K. (2017). Aggregated residual transformations for deep neural networks. In *Proceedings of the IEEE conference on computer vision and pattern recognition*, pages 1492–1500.

Yu, J., Jiang, Y., Wang, Z., Cao, Z., and Huang, T. (2016). Unitbox: An advanced object detection network. In *Proceedings of the 24th ACM international conference on Multimedia*, pages 516–520.

Zheng, Z., Wang, P., Liu, W., Li, J., Ye, R., and Ren, D. (2020). Distance-iou loss: Faster and better learning for bounding box regression. In *Proceedings of the AAAI Conference on Artificial Intelligence*, volume 34, pages 12993–13000.

Zhu, C., He, Y., and Savvides, M. (2019a). Feature selective anchor-free module for single-shot object detection. In *Proceedings of the IEEE/CVF Conference on Computer Vision and Pattern Recognition*, pages 840–849.

Zhu, X., Cheng, D., Zhang, Z., Lin, S., and Dai, J. (2019b). An empirical study of spatial attention mechanisms in deep networks. In *Proceedings of the IEEE/CVF International Conference on Computer Vision*, pages 6688–6697.

APPENDIX

Further results from training the anchor-free dense model over the OPEDD dataset and the COCO benchmark dataset are presented in this Appendix. These results show more information about using different IoU loss functions without the plugin spatial attention as well as with the integration of such an attention mechanism.

Appendix A

Results of training different backbones of FSAF and FCOS models over the COCO dataset are mentioned. Table 6 shows the results of the training FSAF model with different IoU loss without an attention mechanism in part (a) as well as with an attention mechanism in part (b). Table 7 shows the same but for the FCOS model.

Appendix B

FSAF and FCOS models based on different backbones are investigated with and without spatial attention mechanism. Those models are trained over a specific OPEDD dataset. Table 8 and Table 9 show detailed results, which express that using another regression loss rather than IoU improves the accuracy of the models.

Table 6: Ablation studies for the FSAF model trained on COCO dataset using different structures of backbones, loss types and attention.

(a) FSAF model structure with different loss types without using an attention mechanism.

Model	Backbone	loss	bbox-mAP	bbox-mAP-50	bbox-mAP-75	bbox-mAP-s	bbox-mAP-m	bbox-mAP-l
FSAF	ResNet-50	IoU [lit]	36.0	55.5	37.7	19.6	39.6	**48.2**
		CIoU	**36.8**	**55.7**	**38.9**	**19.8**	**39.7**	48.0
		DIoU	35.3	54.1	37.4	19.2	37.9	46.0
		GIoU	35.2	54.0	37.3	18.9	37.8	45.9
FSAF	ResNet-101	IoU [lit]	**39.3**	**58.6**	**42.1**	**22.1**	**43.4**	**51.2**
		CIoU	38.5	57.7	41.0	20.6	41.7	50.2
		DIoU	38.7	57.9	41.0	20.9	42.2	**51.2**
		GIoU	38.6	57.6	41.1	21.6	42.4	50.7
FSAF	ResNeXt-101	IoU [lit]	**42.4**	**62.5**	**45.5**	**24.6**	**46.1**	**55.5**
		CIoU	41.3	60.9	44.1	23.3	45.0	54.2
		DIoU	41.4	61.1	44.6	23.5	45.1	54.7
		GIoU	41.2	60.8	44.2	23.0	45.1	53.6

(b) FSAF model structure with different loss types and using an attention mechanism.

Model	Backbone	att	Loss	bbox-mAP	bbox-mAP-50	bbox-mAP-75	bbox-mAP-s	bbox-mAP-m	bbox-mAP-l
FSAF	ResNet-50	ε3	IoU	36.3	55.4	38.6	20.1	39.4	47.7
			CIoU	**37.3**	56.8	39.2	21.1	40.0	**49.0**
			DIoU	**37.3**	**56.9**	39.2	**21.2**	**40.1**	48.6
			GIoU	37.2	56.4	**39.6**	21.0	40.0	**49.0**
FSAF	ResNet-101	ε3	IoU	37.8	57.0	40.2	21.3	41.5	49.3
			CIoU	40.0	**59.9**	**42.7**	22.4	43.8	52.0
			DIoU	**40.1**	59.7	**42.7**	**22.5**	**44.0**	52.3
			GIoU	39.8	59.3	42.3	**22.5**	43.3	**52.4**
FSAF	ResNeXt-101	ε3	IoU	42.4	62.8	45.3	24.5	46.4	55.5
			CIoU	40.2	59.9	42.8	22.9	43.7	52.3
			DIoU	**43.0**	**63.5**	**46.1**	**25.5**	**46.9**	**56.6**
			GIoU	42.5	62.7	45.6	24.5	46.3	56.1

Table 7: Ablation studies on FCOS model trained on COCO dataset using different structures of backbones, loss types and attention.

(a) FCOS model structure with different loss types without using an attention mechanism.

Model	Backbone	loss	bbox-mAP	bbox-mAP-50	bbox-mAP-75	bbox-mAP-s	bbox-mAP-m	bbox-mAP-l
FCOS	ResNet-50	IoU [lit]	36.6	**56.0**	38.8	**21.1**	40.7	47.1
		CIoU	36.7	55.3	39.0	20.0	40.7	47.3
		DIoU	**37.0**	55.6	**39.5**	21.0	40.6	**47.9**
		GIoU	37.0	55.5	39.4	**21.1**	**40.9**	47.5
FCOS	ResNet-101	IoU [lit]	39.1	**58.3**	**42.1**	22.7	43.3	50.3
		CIoU	38.8	57.53	41.3	22.42	42.86	50.23
		DIoU	39.08	58.04	41.77	22.31	43.07	**50.46**
		GIoU	**39.22**	58.16	42.02	**22.79**	**43.47**	50.06
FCOS	ResNeXt-101	IoU [lit]	42.6	62.3	45.6	25.7	46.3	54.6
		CIoU	42.87	**62.35**	46.16	26.89	**46.70**	54.66
		DIoU	**43.04**	62.28	46.22	26.85	46.59	**55.02**
		GIoU	42.85	62.19	**46.48**	**26.94**	46.60	53.94

(b) FCOS model structure with different loss types and using an attention mechanism.

Model	Backbone	att	Loss	bbox-mAP	bbox-mAP-50	bbox-mAP-75	bbox-mAP-s	bbox-mAP-m	bbox-mAP-l
FCOS	ResNet-50	ε3	IoU	37.4	56.3	40.0	21.6	41.1	49.0
			CIoU	**38.2**	**57.1**	**40.6**	21.5	**42.1**	**50.0**
			DIoU	37.8	56.8	40.2	22.0	41.7	49.4
			GIoU	38.1	56.9	40.5	**22.3**	41.9	49.7
FCOS	ResNet-101	ε3	IoU	39.50	58.30	42.46	22.58	43.40	51.90
			CIoU	39.87	58.97	42.57	**23.23**	**43.99**	51.84
			DIoU	**40.07**	**59.14**	**43.12**	23.18	43.89	51.77
			GIoU	39.91	59.03	42.50	23.13	43.89	**51.95**
FCOS	ResNeXt-101	ε3	IoU	43.4	63.2	46.6	26.8	47.4	55.2
			CIoU	**43.8**	**63.3**	**47.2**	**27.5**	**47.8**	56.0
			DIoU	43.3	62.8	46.6	26.9	47.0	55.1
			GIoU	43.7	63.0	47.0	26.6	47.7	**56.5**

Table 8: The results of training the FSAF model on the OPEDD dataset, pretrained on the COCO dataset with different structures of backbones, loss types and attention.

(a) FSAF model structure with different loss types without using an attention mechanism.

Model	Backbone	loss	bbox-mAP	bbox-mAP-50	bbox-mAP-75	bbox-mAP-s	bbox-mAP-m	bbox-mAP-l
FSAF	ResNet-50	IoU [lit]	24.1	35.9	26.8	6.7	41.1	31.6
		CIoU	24.6	38.0	26.7	**8.4**	**43.7**	30.1
		DIoU	24.7	**40.1**	26.5	6.0	38.5	31.8
		GIoU	**25.1**	39.2	**28.0**	7.5	41.1	**31.9**
FSAF	ResNet-101	IoU [lit]	24.6	37.3	28.0	**6.8**	38.2	32.2
		CIoU	**25.4**	37.6	28.0	5.7	**41.6**	**33.7**
		DIoU	25.3	**38.0**	**28.7**	5.2	40.6	33.2
		GIoU	25.1	37.2	27.4	5.3	40.4	33.5
FSAF	ResNeXt-101	IoU [lit]	26.3	**40.1**	28.9	8.0	41.1	34.4
		CIoU	**27.5**	**40.1**	**30.0**	**9.6**	41.8	**36.0**
		DIoU	26.9	39.5	**30.0**	6.9	43.4	34.3
		GIoU	26.6	39.4	29.7	6.4	**45.9**	33.9

(b) FSAF model structure with different loss types and using an attention mechanism.

Model	Backbone	att	Loss	bbox-mAP	bbox-mAP-50	bbox-mAP-75	bbox-mAP-s	bbox-mAP-m	bbox-mAP-l
FSAF	ResNet-50	ε3	IoU	**24.5**	**38.2**	25.5	7.6	39.5	**32.0**
			CIoU	24.1	37.4	26.5	**9.2**	40.7	30.5
			DIoU	23.4	35.7	24.7	6.1	**42.0**	29.0
			GIoU	**24.5**	37.3	**26.8**	7.9	38.4	31.8
FSAF	ResNet-101	ε3	IoU	24.6	**38.7**	25.8	5.1	**40.1**	32.8
			CIoU	24.0	36.7	25.3	5.6	39.8	31.8
			DIoU	**24.8**	36.9	**26.8**	4.7	37.4	**33.4**
			GIoU	24.5	38.5	25.7	**7.5**	39.6	31.8
FSAF	ResNeXt-101	ε3	IoU	26.7	41.0	29.2	8.1	41.6	34.3
			CIoU	26.8	**41.4**	29.4	7.1	41.4	34.4
			DIoU	26.3	40.0	30.2	8.2	**44.7**	33.6
			GIoU	**26.9**	40.2	**30.3**	**8.4**	41.4	**34.9**

Table 9: The results of training the FCOS model on the OPEDD dataset, pre-trained on coco dataset with different structures of backbones, loss types and attention.

(a) FCOS model structure with different loss types without using an attention mechanism.

Model	Backbone	loss	bbox-mAP	bbox-mAP-50	bbox-mAP-75	bbox-mAP-s	bbox-mAP-m	bbox-mAP-l
FCOS	ResNet-50	IoU [lit]	24.9	37.0	25.9	3.4	38.2	34.1
		CIoU	25.4	**39.6**	25.8	**4.8**	37.7	33.9
		DIoU	25.4	37.9	**28.1**	4.1	39.3	35.1
		GIoU	**25.8**	38.3	26.9	4.3	**39.7**	**35.5**
FCOS	ResNet-101	IoU [lit]	23.0	36.5	24.9	5.1	36.7	30.7
		CIoU	23.6	37.2	25.0	**5.2**	37.8	32.0
		DIoU	23.9	**38.3**	23.6	3.4	36.4	32.1
		GIoU	**25.1**	37.1	**27.2**	3.2	**40.8**	**33.6**
FCOS	ResNeXt-101	IoU [lit]	24.0	37.1	25.2	**6.4**	37.8	31.3
		CIoU	25.1	37.1	28.1	6.0	**40.1**	32.7
		DIoU	**26.5**	**38.7**	**28.4**	5.4	39.6	**35.1**
		GIoU	25.1	38.1	26.2	**6.4**	38.9	32.1

(b) FCOS model structure with different loss types and using an attention mechanism.

Model	Backbone	att	Loss	bbox-mAP	bbox-mAP-50	bbox-mAP-75	bbox-mAP-s	bbox-mAP-m	bbox-mAP-l
FCOS	ResNet-50	ε3	IoU	23.7	36.3	25.8	3.1	35.7	32.5
			CIoU	24.8	37.8	26.8	3.9	37.3	34.2
			DIoU	25.4	**39.2**	**27.1**	**4.7**	38.1	**34.9**
			GIoU	**25.6**	**39.2**	26.9	**4.7**	**39.9**	34.6
FCOS	ResNet-101	ε3	IoU	23.4	35.6	25.2	**4.9**	37.3	31.5
			CIoU	**24.4**	**38.7**	24.8	3.9	36.8	**33.6**
			DIoU	23.8	37.9	24.2	4.5	**37.6**	31.9
			GIoU	23.5	36.1	**25.8**	4.5	37.1	32.6
FCOS	ResNeXt-101	ε3	IoU	**26.1**	**38.7**	**28.5**	4.2	42.3	34.3
			CIoU	25.0	37.8	26.1	**6.0**	38.2	33.1
			DIoU	25.5	37.5	26.5	4.1	38.6	**34.4**
			GIoU	26.0	37.5	27.3	5.3	**42.9**	33.8